coatings

MDPI

Article

$CoMoO_4$ Nanoflowers Doped with La Element for Advanced Electrode Materials

Donghua Chen *, Yang Liu, Danting Li, Tenghao Ma and Jing Wang

School of Light Industry, Harbin University of Commerce, Harbin 150028, China; ly760576542@163.com (Y.L.); ldtjing@sina.com (D.L.); 18234590846@163.com (T.M.); wangwangmayong@126.com (J.W.)
* Correspondence: 102959@hrbcu.edu.cn

Abstract: La-$CoMoO_4$ was prepared as the electrode material for supercapacitors using the freeze-drying method. The physical and structural properties of the prepared electrode La-$CoMoO_4$ were characterized by scanning electron microscopy (SEM) and transmission electron microscopy (TEM). We further investigated the electrochemical performance of La-$CoMoO_4$ electrode materials through cyclic voltammetry, constant current charge–discharge, and electrochemical impedance spectroscopy. The research results indicate that compared with $CoMoO_4$ material (1400 F/g), La-$CoMoO_4$ material has a high specific capacitance of 2248 F/g at a current density of 1 A/g. In addition, La-$CoMoO_4$ has a high stability, with a capacitance retention rate of up to 99.2% after 5500 cycles. Finally, supercapacitor devices using La-$CoMoO_4$ material as the positive electrode have a high energy density of 55 Wh/Kg (power density of 1000 W/Kg), making them a promising electrode material.

Keywords: supercapacitors; electrode materials; freeze drying method; La-$CoMoO_4$ nanoflowers

check for updates

Citation: Chen, D.; Liu, Y.; Li, D.; Ma, T.; Wang, J. $CoMoO_4$ Nanoflowers Doped with La Element for Advanced Electrode Materials. *Coatings* **2024**, *14*, 388. https://doi.org/10.3390/coatings14040388

Academic Editor: Alina Pruna

Received: 4 March 2024
Revised: 19 March 2024
Accepted: 20 March 2024
Published: 27 March 2024

Copyright: © 2024 by the authors. Licensee MDPI, Basel, Switzerland. This article is an open access article distributed under the terms and conditions of the Creative Commons Attribution (CC BY) license (https://creativecommons.org/licenses/by/4.0/).

1. Introduction

With the evolution of the times, human demand for energy is increasing day by day. With the advancement of industrialization, resources are becoming rapidly depleted, and environmental problems are becoming increasingly serious [1–4]. As an economical and clean energy source, electricity can be applied in many situations, but it has the disadvantage of being difficult to store. Therefore, people need to search for low-cost and high-efficiency energy storage devices [5–8]. Supercapacitors are considered one of the most promising energy storage devices in the energy field due to their high power density, fast charging and discharging, green environmental protection, and long service life [9–15]. The low energy density has limited the development and application of capacitors and is also the main factor affecting their performance [16–19]. According to the energy density $E = 1/2CV^2$, it can be found that the specific capacitance (C) and voltage window (V) directly affect the energy density. Therefore, we can develop excellent electrode materials through experimental development to improve the specific capacitance (C) and enhance the energy density of supercapacitors [20–23]. In addition to developing excellent electrode materials, asymmetric supercapacitors can also be assembled by using two different electrode materials, which can expand the voltage window and thereby improve the energy density [24–27]. At present, the optimization of electrode materials has become a worldwide research hotspot.

Cobalt molybdate, as an electrode material for capacitors, has a high conductivity, cycling stability, redox activity, and good rate performance [28–30]. It is a promising electrode material, but it is not as good at capacitance. To overcome these problems, researchers have made many attempts, such as designing nanostructures, doping elements, etc., to improve the performance of the products. The current main research focus is on creating nanomaterials with distinctive structures. Wang et al. [31]. successfully synthesized a $CoMoO_4$ nanowire array using the hydrothermal method. The material has a specific

capacity of 940 F/g at a current density of 1 A/g. Using this material as the positive electrode and activated carbon (AC) as the negative electrode, this asymmetric supercapacitor device has a maximum voltage of 1.6 V, energy density of 46.7 Wh/kg, and power density of 8000 W/kg. In addition, element doping also greatly improves the performance of materials. Doping rare earth elements can alter the binding strength of electrode materials, the local environment of the lattice, and the valence state of cations, thereby introducing defects and increasing oxygen vacancies in electrode materials. The introduction of defects can change the disordered state inside atoms, adjust the size of ion transport channels, improve conductivity, and oxygen-rich vacancies can act as active sites to absorb more OH^- and accelerate surface reaction kinetics, thereby improving electrochemical performance. This has a positive significance in solving the problem of slow reaction kinetics and increasing material specific capacity [32,33]. Theerthagiri et al. [34] doped a series of Co_3O_4 materials with rare earth metals (La, Nd, Gd, Sm) and found that compared to pure Co_3O_4 materials, the specific capacitance of the products increased from 656.2 F/g to 2193 F/g, while also exhibiting good cycling stability. After 5000 cycles, the capacitance retention rate was 93.18%.

This article uses a simple and low-cost freeze-drying method to modify $CoMoO_4$ materials with rare earth element La, and successfully prepares La-$CoMoO_4$ nanoflower structures with large specific surface areas. The materials are characterized by various characterization methods, and the results show that La-$CoMoO_4$ materials have a unique three-dimensional flower-like structure. Through electrochemical performance testing, La-$CoMoO_4$ material has a high specific capacitance of 2248 F/g at a current density of 1 A/g. After 5500 cycles, the capacitance retention rate reached 99.2%. We further assembled the supercapacitor device using La-$CoMoO_4$ material as the positive electrode and CNTs as the negative electrode. The device has a high specific capacity of 149 F/g at a current density of 1 A/g and a high energy density of 55 Wh/Kg (power density of 1000 W/Kg), and it exhibits a superior electrochemical performance compared to the original $CoMoO_4$ material. This article provides a reference value for the application of rare earth elements in electrode materials.

2. Materials and Methods

2.1. Preparation of $CoMoO_4$ Material

Add 1.5 mmol of $Co(NO_3)_2 \cdot 6H_2O$ and 3 mmol of $Na_2MoO_4 \cdot 7H_2O$ into 30 mL of deionized water, stir the solution evenly, put 1 cm^2 of foam nickel into the beaker, and continue stirring for 2 h. Put the stirred solution into a high-pressure reactor for hydrothermal reaction, adjust the temperature to 60 °C, and adjust the time to 24 h. Then, remove the product and repeatedly clean it with deionized water. Freeze-dry the cleaned sample for 24 h, and finally calcine it in the air at 400 °C and 1 °C/min for 5 h to obtain $CoMoO_4$ nanoflowers.

2.2. Preparation of La-$CoMoO_4$ Material

Repeat the step of preparing $CoMoO_4$ in step 1.1, add lanthanum acetate solution to the above solution, continue to stir evenly, put 1 cm^2 foam nickel into the beaker, and continue to stir for 2 h. Put the stirred solution into a high-pressure reactor for hydrothermal reaction, adjust the temperature to 60 °C, and adjust the time to 24 h. Then, remove the product and repeatedly clean it with deionized water. Freeze-dry the cleaned sample for 24 h, and finally calcine it in the air at 400 °C and 1 °C/min for 5 h to obtain La-$CoMoO_4$ nanoflowers (Figure 1).

2.3. Preparation of CNTs Electrode Materials

References on the preparation of carbon nanotubes [35,36].

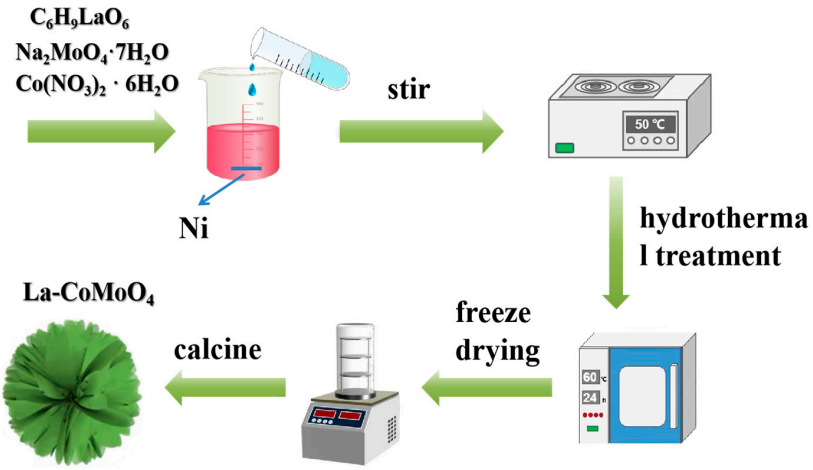


Figure 1. Schematic diagram of the preparation process of La-$CoMoO_4$ material.

2.4. Assembly of Components

A supercapacitor was assembled using La-$CoMoO_4$ nanoflower structure material as the positive electrode, carbon nanotubes (CNTs) as the negative electrode, and KOH as the electrolyte. The area of the positive and negative electrode materials is 1 cm^2. Mix 2.8 g KOH and 3 g PVA into 5 mL deionized water to prepare the gel electrolyte. Dip the electrode materials and separator into the electrolyte mentioned above, take them out after 5 min, assemble them, and place them in the air for curing. Dry the device under vacuum conditions for 24 h to obtain La-$CoMoO_4$/Ni//CNTs/Ni asymmetric devices, as shown in Figure 2.

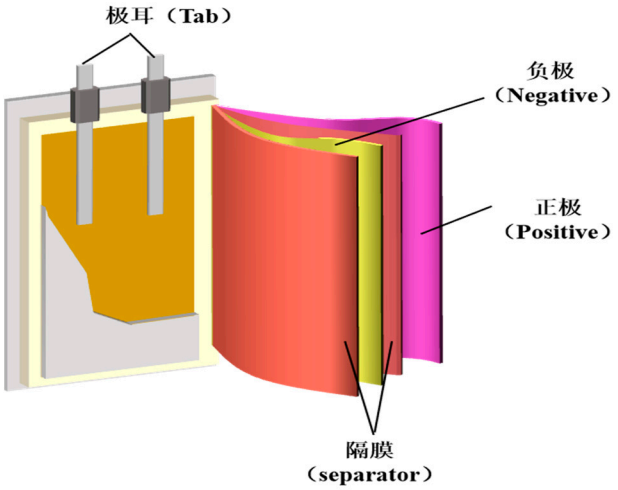


Figure 2. Schematic diagram of supercapacitor device.

2.5. Material Characterization

Observe the morphological characteristics of the sample material using scanning electron microscopy (SEM) and transmission electron microscopy (TEM, JEOL JEM-2100 F). The cyclic voltammetry (CV) test is conducted within the potential range of −0.2 to 0.6 V (relative to SCE). The constant current charging/discharging test is conducted at various current densities within the potential range of 0–0.5 V (relative to SCE). An electrochemical impedance spectroscopy (EIS) measurement is performed by applying an alternating voltage with an amplitude of 5 mV and a frequency range of 0.1 Hz to 100 kHz at an open circuit potential. Element distribution and energy dispersive X-ray spectroscopy tests were conducted on Hitachi S-4800 scanning electron microscopy, transmission electron microscopy (TEM), and high-resolution HRTEM. The structures of the samples were characterized by X-ray diffraction (XRD, Rigaku D/max-rB, CuKa radiation, =0.1542 nm, 40 kV, 100 mA).

An FD-1C-5 instrument is required in the material preparation process. Electrochemical testing was conducted on the CHI660E electrochemical workstation at Shanghai Chenhua, and the relevant calculation formulas involved in the article are as follows:

$$q = Cs \times \Delta v \times m \tag{1}$$

$$m+/m- = c- \times \Delta v - /c+ \times \Delta v+ \tag{2}$$

$$Cs = I\Delta t/m\Delta v \tag{3}$$

$$p = 3600E/\Delta t \tag{4}$$

Cs (specific capacitance, F/g), I (discharge current, A), ΔT (discharge time, s), ΔV (voltage difference, v), m (mass of active material, g).

3. Results and Discussion

We conducted scanning tests on the experimentally prepared La-$CoMoO_4$ nanoflower material and observed its microstructure. Figure 3a shows the SEM image of the foam Ni substrate, which shows that a large number of closely arranged La-$CoMoO_4$ materials are attached to the Ni substrate. We observed these materials at a low magnification and found that these tightly arranged La-$CoMoO_4$ materials exhibit a nanoflower-like structure, as shown in Figure 3b. To observe the microstructure of La-$CoMoO_4$ nanoflower material more clearly, it was further observed at a high magnification, as shown in Figure 3c. The figure shows that the nanoflower is composed of a large number of sheet-like structures growing in different directions, interweaving to form a nanoflower structure. We further conducted SEM mapping tests on the selected area in Figure 3c, as shown in Figure 3f, which showed the following four elements: Co, Mo, O, and La. The microstructure of the material plays an important role in its electrochemical performance, and we further conducted TEM testing on the material. As shown in Figure 3d, the TEM image of La-$CoMoO_4$ material shows that the flower-like structure is composed of ultra-thin nanosheets, which is consistent with the SEM test results in the above figure. Figure 3e shows a high-power TEM image of the La-$CoMoO_4$ flower-like structure material, with a lattice spacing of 0.336 nm, corresponding to the (002) lattice plane of La-$CoMoO_4$. The inset in the figure shows the selected electron diffraction pattern, which shows that the material is polycrystalline. We also conducted TEM mapping tests on the prepared materials, as shown in Figure 3g, indicating that the prepared materials contain the following four elements: Co, Mo, O, and La.

Figure 4a shows the elemental analysis test of La-$CoMoO_4$ material. It can be seen from the figure that the flower-shaped structure material contains four elements, La, Co, Mo, O, and no other elements. Figure 4b shows the XRD pattern of La-$CoMoO_4$ material, where $CoMoO_4$ is a monoclinic phase of $CoMoO_4$ (PDF, card No. 21-0868). The spectrum contains several weak diffraction peaks, namely $CoMoO_4 \cdot 0.9H_2O$. After doping with the rare earth element La, the diffraction peak of the product La-$CoMoO_4$ shifts slightly to the left, and the intensity slightly decreases. This is because the doping element reduces the crystallinity and disorder of the product, causing lattice distortion. The above experimental tests indicate that the La-$CoMoO_4$ material has been successfully prepared.

To further investigate the effect of La doping on the morphology of materials, the specific surface areas of the experimentally prepared $CoMoO_4$ and La-$CoMoO_4$ materials were further analyzed through N^2 adsorption–desorption curves and pore size distribution curves. As shown in Figure 5a, the test results show that the specific surface area of the $CoMoO_4$ flower-like structure material is 98.82 m^2/g, and the pore size distribution is around 27 nm. Figure 5b shows that the specific surface area of the La-$CoMoO_4$ flower-like structure material is 126.7 m^2/g, with a pore size distribution of around 27 nm. After comparison, it was found that the pore size of the material did not change significantly before and after doping, while the specific surface area of the material increased after doping. La-$CoMoO_4$ material has abundant pores and a large specific surface area, providing more electrochemical reaction sites for the reaction, allowing the electrolyte to be fully distributed

on the electrode surface, shortening the ion transport path, and thereby accelerating the electrochemical rate and improving the electrochemical performance.

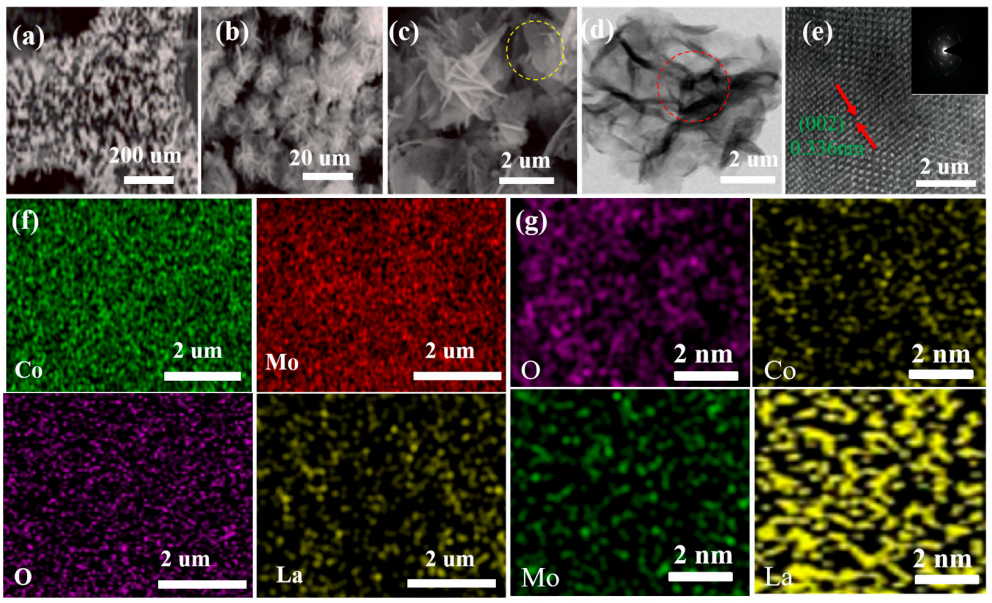


Figure 3. (**a**) SEM image of La-$CoMoO_4$ nanowire; SEM images of self-supporting La-$CoMoO_4$ nanoflower-structured nanomaterials under different magnification conditions (**b**,**c**); (**d**) the TEM image of La-$CoMoO_4$ nanoflower structure; (**e**) HRTEM images of La-$CoMoO_4$ nanoflower structure, illustrated by corresponding electron diffraction patterns; (**f**) SEM mapping of Co, Ni, Mo, and O; (**g**) TEM mapping spectra of Co, Ni, Mo, and O, respectively.

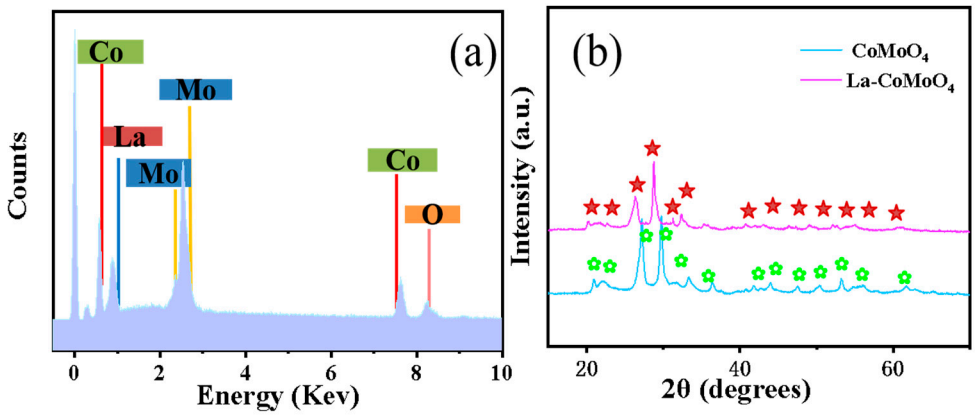


Figure 4. (**a**) The EDS plot of La-$CoMoO_4$; (**b**) XRD pattern of La-$CoMoO_4$ material.

We further investigated the surface chemical composition and the percentage of samples obtained by elemental composition. The samples were characterized and analyzed by XPS test method, and the presence of Mo3d, O 1s, Co2p and La 3d peaks is shown in Figure 6.

We conducted electrochemical testing of Ni, $CoMoO_4$, and La-$CoMoO_4$ flower-shaped nanomaterials. As shown in Figure 7a, at a scanning rate of 5 mV/s, the CV curves of Ni, $CoMoO_4$, and La-$CoMoO_4$ samples are determined by the size of the sample enclosure area. Among the three samples, La-$CoMoO_4$ has the largest area enclosed by the CV curve, indicating the best electrochemical performance. The area enclosed by foam nickel is almost zero, so the influence on the capacitive performance of the material is negligible. Figure 7b shows the charge–discharge curves of three materials. La-$CoMoO_4$ nano-cosmetic material has a longer discharge time compared to Ni and $CoMoO_4$. Based on Figure 7b, we further obtained the specific capacitances of the three samples, which are 40, 1400, and 2248 F/g.

After comparing the specific capacitances of the three samples, it can be seen that the La-$CoMoO_4$ flower-shaped nanostructure material has a better capacitance performance, as shown in Figure 7c. We selected the La-$CoMoO_4$ flower-shaped nanomaterial with the best electrochemical performance among the three materials for further electrochemical testing. Figure 7d shows the CV curves of La-$CoMoO_4$ material at different scanning speeds. With the increase in scanning speed, the peak current increases, and the area enclosed by the curve gradually increases, indicating that the reaction process accelerates and the charge storage capacity increases. As the scanning rate increases, there is no significant change in the curve shape, indicating that the La-$CoMoO_4$ material has a good stability. Figure 7e shows the charge–discharge curves at densities of 1, 3, 5, 8, 10, and 12 A/g under different currents. According to the formula, the corresponding specific capacities are calculated to be 2248, 2160, 1930, 1860, 1780, and 1698 F/g, as shown in Figure 7f.

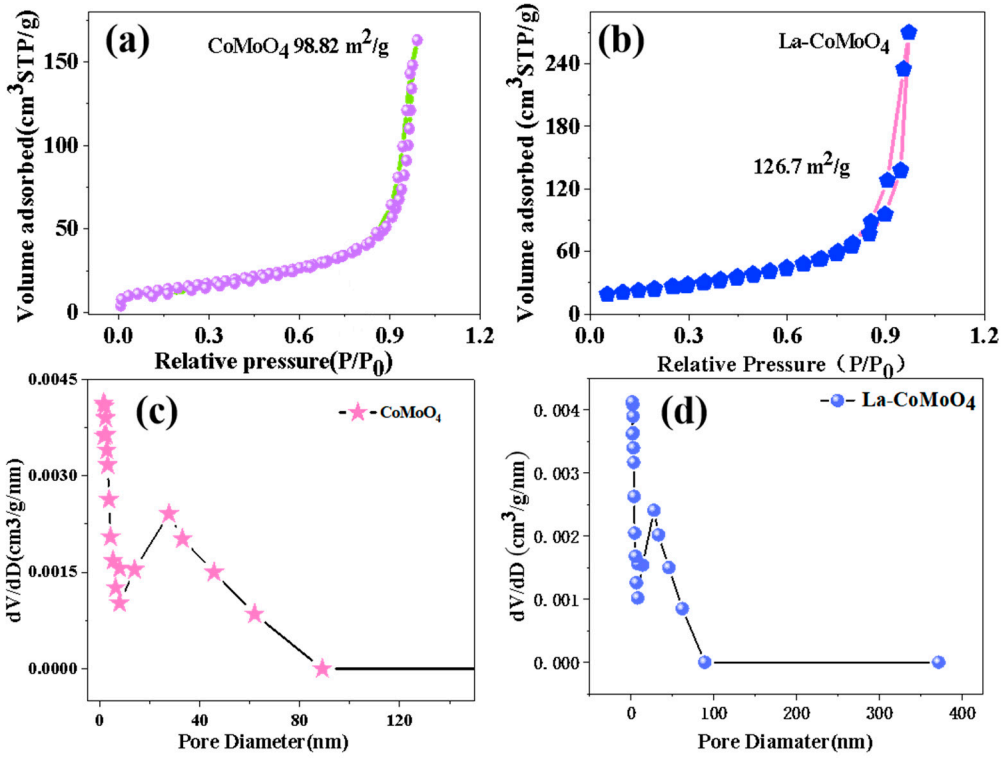


Figure 5. (**a**,**c**) The N_2 adsorption–desorption curve and pore size distribution curve of $CoMoO_4$; (**b**,**d**) the N_2 adsorption–desorption curve and pore size distribution curve of La-$CoMoO_4$.

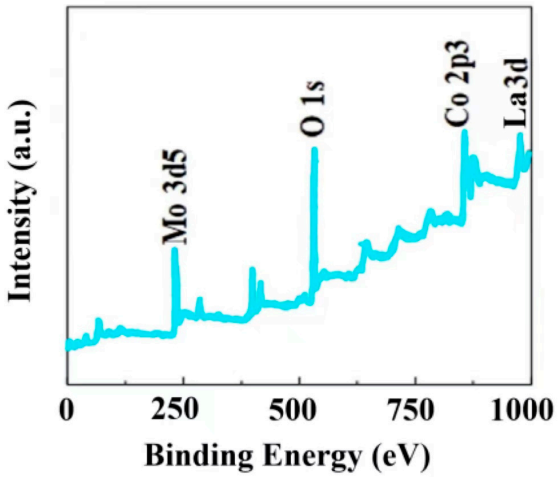


Figure 6. XPS spectra of La-$CoMoO_4$.

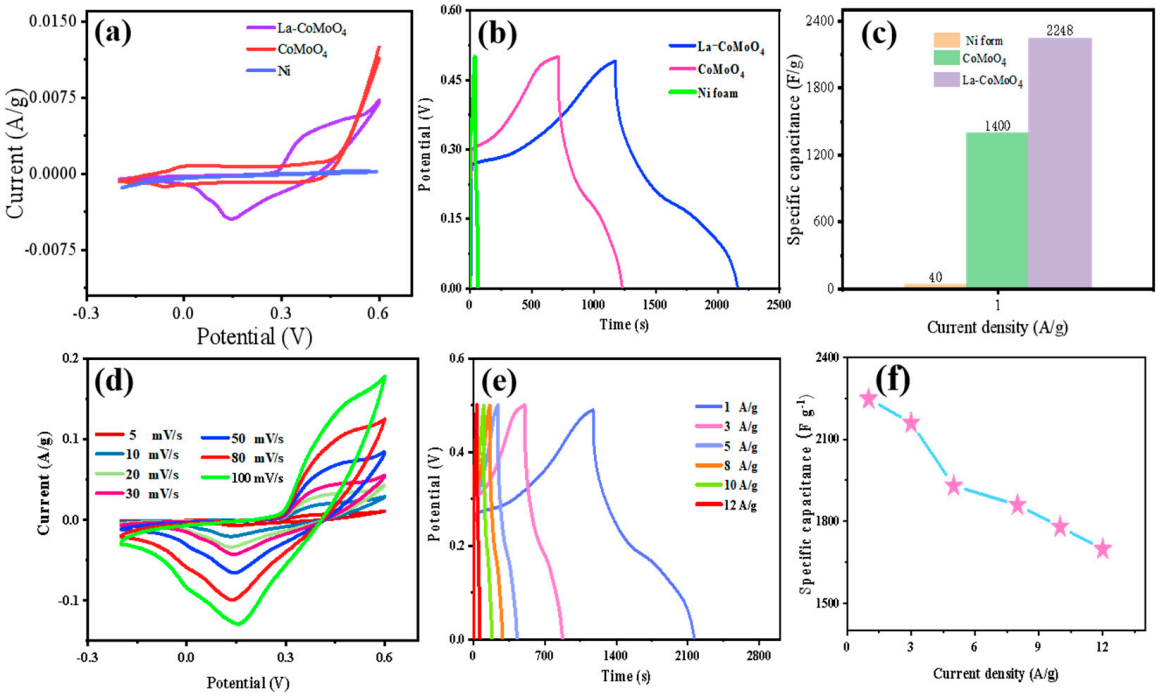


Figure 7. (**a**) The CV curves of Ni, $CoMoO_4$, and La-$CoMoO_4$ at 4 mV/s; (**b**) GCD curves of Ni, $CoMoO_4$, and La-$CoMoO_4$ at a current density of 4 A/g; (**c**) the specific capacity diagrams of Ni, $CoMoO_4$, and La-$CoMoO_4$ at 1 A/g; (**d**) CV curves of La-$CoMoO_4$ at different scanning rates; (**e**) GCD curves of La-$CoMoO_4$ under different current densities; (**f**) Specific Capacity Diagram of La-$CoMoO_4$ materials at different current densities.

We further conducted cyclic stability tests on La-$CoMoO_4$ material at a current density of 1 A/g. After 5500 cycles, the specific capacity decreased from 2248 F/g to 2229 F/g, with a specific capacity retention rate of 99.2%. The material exhibited an excellent cyclic stability performance, as shown in Figure 8a. Figure 8b shows the impedance comparison between the first and 5500th cycles of the La-$CoMoO_4$ nanoflower material. It can be seen that the diffusion resistance slightly increases after 5500 cycles, which is due to the detachment of the active material and its inability to fully reflect with the electrolyte after 5500 cycles.

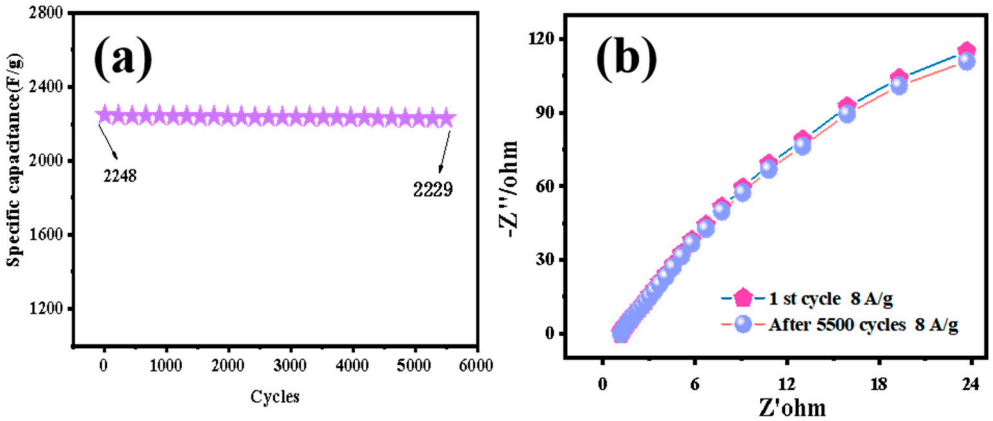


Figure 8. (**a**) Cyclic performance of La-$CoMoO_4$ material at a current density of 1 A/g; (**b**) Nyquist diagram of La-$CoMoO_4$ material.

Figure 9a shows the change in the specific capacity of La-$CoMoO_4$ material after continuously changing the current density and returning to the initial current. When the initial current is 8 A/g, the specific capacity is 1860 F/g. After multiple changes in current density and returning to the initial current of 8 A/g, the specific capacity is 1856 F/g and

the capacitance retention rate is 99.8%. There is no significant attenuation in the specific capacity, and the material exhibits a good rate performance and stability. Figure 9b shows the schematic diagram of the reaction between the nanoflower-structure electrode material and ions and electrons. The La-$CoMoO_4$ electrode material has an excellent electrochemical performance for the following reasons: foam nickel itself has good conductivity, and porous foam nickel is conducive to the diffusion of electrolyte on its surface; La-$CoMoO_4$ is directly grown on the foam nickel substrate, reducing the influence of adhesive on conductivity; the flower-like structure increases the specific surface area of the electrode material, which is conducive to full contact between ion electrons and the electrode material and improves the progress of chemical reactions. We will compare the specific capacity of the prepared La-$CoMoO_4$ material with other works, as shown in Table 1.

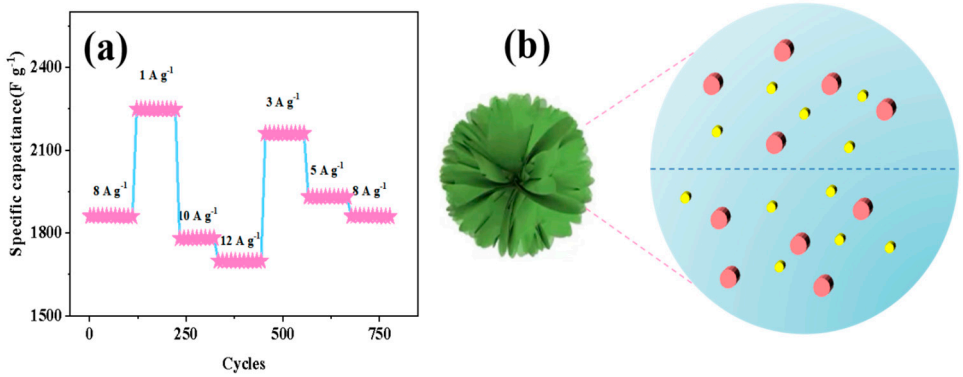


Figure 9. (**a**) Rate and periodic performance of La-$CoMoO_4$ material under different current densities; (**b**) corresponding reaction mechanism diagram.

Table 1. Comparison of electrode material properties with the literature.

Electrode Material	Current Density [1 A/g]	Specific Capacitance [F/g]	Number of Cycles	Capacity Retention Rate (%)	Ref
KCu_7S_4@$NiMoO_4$	1	1194.6	10,000	92.3%	[34]
$NiMoO_4$@Mg-Co(OH)F/NF	1	1630	6000	86%	[35]
$NiCo_2S_4$@$NiMoO_4$	5	1447	10,000	88%	[36]
CNTs/$NiMoO_4$	20	727.2	2000	86.8%	[37]
La-$CoMoO_4$	1	2248	5500	99.2%	this work

Figure 10a shows the cyclic voltammetry curves of the La-$CoMoO_4$ positive electrode and CNTs negative electrode under a three-electrode testing system with a scanning rate of 5 mV/s. The potential window of La-$CoMoO_4$ is −0.2–0.6 V, and that of carbon nanotubes is −1.0–0.0 V. The voltage window of the asymmetric supercapacitor device assembled with two materials is the difference between the positive and negative voltage windows, so the theoretical voltage window of the asymmetric device assembled with two materials is −1.0–0.6 V. We placed the experimentally assembled La-$CoMoO_4$/Ni//CNTs/Ni supercapacitor device in a two-electrode system and conducted performance tests at a scanning rate of 5 mV/s. Figure 10b shows the cyclic voltammetry test curves of the device at different voltages of 0.8, 1.0, 1.2, 1.4, and 1.6 V and a scanning rate of 5 mV/s. It can be seen from the figure that there is no significant change in the cyclic voltammetry curve when the voltage window is 0–1.6. Further experiments were conducted to test the cyclic voltammetry curves of La-$CoMoO_4$/Ni//CNTs/Ni devices at different scanning rates of 10, 30, 50, 80, and 100 mV/s with a voltage window of 1.6 V, as shown in Figure 10c. As the scanning rate gradually increases, the peak current gradually increases, and the area enclosed by the curve also gradually increases, indicating that the material has a good capacitive performance. When the scanning rate increased to 100 mV/s, the curve shape did not change, indicating that the material has good stability. Next, we will conduct

charge–discharge tests on the device, as shown in Figure 10d. The curve has good symmetry, proving that the device has good stability within the test voltage range. Figure 10e shows the specific capacities of the device calculated based on the GCD curve at different currents of 1, 3, 5, 8, 10, and 12 A/g, with capacities of 149, 125, 113, 109, 102, and 99 F/g. Figure 10f shows the energy comparison of La-$CoMoO_4$/Ni//CNTs/Ni devices. When the current density is 1 A/g, the power density of the device is 1000 W/kg and the energy density is 55 Wh/kg. Compared with the performance of devices in other studies, it has a better performance [38–41].

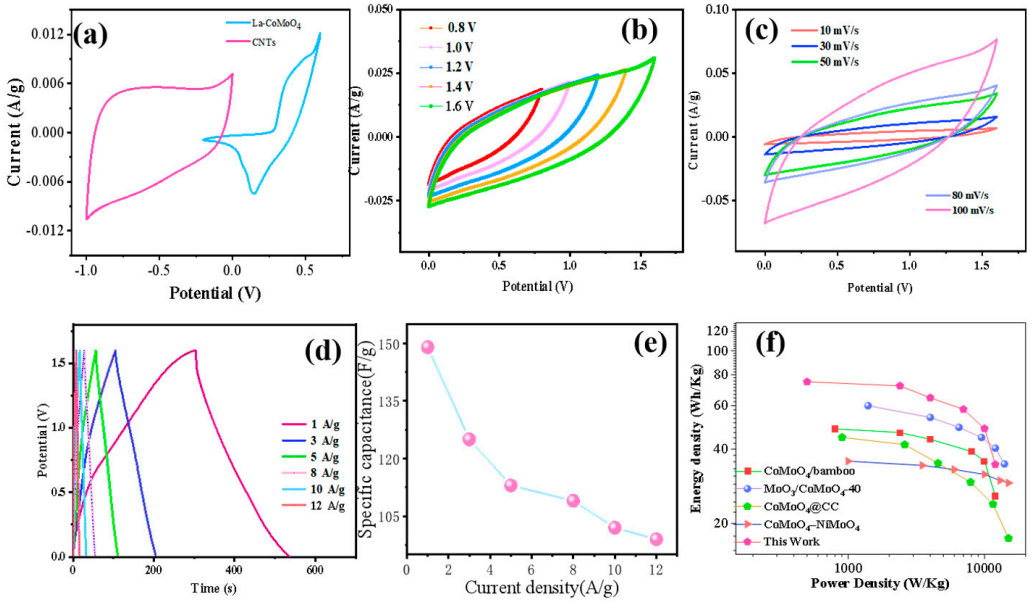


Figure 10. (**a**) CV curves of La-$CoMoO_4$ and CNTs at 4 mV/s; (**b**) CV curves of La-$CoMoO_4$//CNTs at different voltages; (**c**) CV curves of La-$CoMoO_4$//CNTs at different scanning rates; (**d**) GCD curves of La-$CoMoO_4$//CNTs under different current densities; (**e**) specific capacity diagram of La-$CoMoO_4$//CNTs; (**f**) Ragone plot of energy density and power density of La-$CoMoO_4$//CNTs compared to other energy storage devices.

4. Conclusions

A La-$CoMoO_4$ nanoflower structure was synthesized using the freeze-drying method, and the microstructure and elemental composition of the material were analyzed by SEM, TEM, XRD, and EDS. The electrochemical properties of $CoMoO_4$ nanoflowers and La-$CoMoO_4$ nanoflower materials were tested and analyzed using CV, GCD, and EIS. The experimental results show that the specific capacitance of the original $CoMoO_4$ nanoflower material is 1400 F/g, and the specific capacitance of the doped La-$CoMoO_4$ nanoflower material is 2248 F/g. We conducted cycling stability tests on La-$CoMoO_4$ nanoflowers, and after 5500 cycles at a current density of 1 A/g, the capacitance retention rate was 99.2%. The energy density of the asymmetric supercapacitor device assembled with La-$CoMoO_4$ nanoflowers as the positive electrode is 55 Wh/Kg (power density 1000 W/Kg), and La-$CoMoO_4$ nanoflowers are valuable electrode materials for applications.

Author Contributions: D.C. and Y.L. explored research ideas and wrote the paper. J.W. provided guidance for the research process. T.M. and D.L. analyzed the experimental results and revised the manuscript. All authors participated in this experimental study. All authors have read and agreed to the published version of the manuscript.

Funding: Basic research business fees for provincial higher education institutions in Heilongjiang Province (2023-KYYWF-1019). National Natural Science Foundation of China (No. 52002099); Fund of State Key Laboratory of Efficient Utilization of Coal and Green Chemical Industry (Grant No. 2022-K74); Heilongjiang Provincial Youth Scientific Research Project (No. 2019DS084).

Institutional Review Board Statement: Not applicable.

Informed Consent Statement: Not applicable.

Data Availability Statement: Under reasonable conditions, it can be obtained from the author.

Conflicts of Interest: The authors declare no conflicts of interest.

References

1. Rahman, M.M.; Oni, A.O.; Gemechu, E.; Kumar, A. Assessment of energy storage technologies: A review. *Energy Convers. Manag.* **2020**, *223*, 11329. [CrossRef]
2. Shen, X.; Zhang, X.-Q.; Ding, F.; Huang, J.-Q.; Xu, R.; Chen, X.; Yan, C.; Su, F.-Y.; Chen, C.-M.; Liu, X.; et al. Advanced electrode materials in lithium batteries: Retrospect and prospect. *Energy Mater. Adv.* **2021**, *2021*, 1205324. [CrossRef]
3. Rajkumar, S.; Gowri, S.; Dhineshkumar, S.; Merlin, J.P.; Sathiyan, A. Investigation on $NiWO_4$/PANI composite as an electrode material for energy storage devices. *New J. Chem.* **2021**, *45*, 20612–20623. [CrossRef]
4. Wang, Y.; Qu, Q.; Gao, S.; Tang, G.; Liu, K.; He, S.; Huang, C. Biomass derived carbon as binder-free electrode materials for supercapacitors. *Carbon* **2019**, *155*, 706–726. [CrossRef]
5. Zhang, Y.Z.; Wang, Y.; Cheng, T.; Lai, W.Y.; Pang, H.; Huang, W. Flexible supercapacitors based on paper substrates: A new paradigm for low-cost energy storage. *Chem. Soc. Rev.* **2015**, *44*, 5181–5199. [CrossRef]
6. Li, H.; Zhang, X.; Zhao, Z.; Hu, Z.; Liu, X.; Yu, G. Flexible sodium-ion based energy storage devices: Recent progress and challenges. *Energy Storage Mater.* **2020**, *26*, 83–104. [CrossRef]
7. Zhang, W.; Liu, H.; Zhang, X.; Li, X.; Zhang, G.; Cao, P. 3D printed micro-electrochemical energy storage devices: From design to integration. *Adv. Funct. Mater.* **2021**, *31*, 2104909. [CrossRef]
8. Xu, T.; Du, H.; Liu, H.; Liu, W.; Zhang, X.; Si, C.; Liu, P.; Zhang, K. Advanced nanocellulose-based composites for flexible functional energy storage devices. *Adv. Mater.* **2021**, *33*, 2101368. [CrossRef] [PubMed]
9. Ding, H.; Zang, W.; Li, J.; Jiang, Y.; Zou, H.; Ning, N.; Tian, M.; Zhang, L. CB/PDMS electrodes for dielectric elastomer generator with low energy loss, high energy density and long life. *Compos. Commun.* **2022**, *31*, 101132. [CrossRef]
10. Song, L.; Zheng, T.; Zheng, L.; Lu, B.; Chen, H.; He, Q.; Zheng, W.; Hou, Y.; Lian, J.; Wu, Y.; et al. Cobalt-doped basic iron phosphate as bifunctional electrocatalyst for long-life and high-power-density rechargeable zinc-air batteries. *Appl. Catal. B Environ.* **2022**, *300*, 120712. [CrossRef]
11. Raza, W.; Ali, F.; Raza, N.; Luo, Y.; Kim, K.H.; Yang, J.; Kumar, S.; Mehmood, A.; Kwon, E.E. Recent advancements in supercapacitor technology. *Nano Energy* **2018**, *52*, 441–473. [CrossRef]
12. Najib, S.; Erdem, E. Current progress achieved in novel materials for supercapacitor electrodes: Mini review. *Nanoscale Adv.* **2019**, *1*, 2817–2827. [CrossRef]
13. Chen, G.Z. Supercapacitor and supercapattery as emerging electrochemical energy stores. *Int. Mater. Rev.* **2017**, *62*, 173–202. [CrossRef]
14. Wang, Y.; Wu, X.; Han, Y.; Li, T. Flexible supercapacitor: Overview and outlooks. *J. Energy Storage* **2021**, *42*, 103053. [CrossRef]
15. Meng, Q.; Cai, K.; Chen, Y.; Chen, L. Research progress on conducting polymer based supercapacitor electrode materials. *Nano Energy* **2017**, *36*, 268–285. [CrossRef]
16. Mevada, C.; Mukhopadhyay, M. Limitations and recent advances in high mass loading asymmetric supercapacitors based on pseudocapacitive materials. *Ind. Eng. Chem. Res.* **2021**, *60*, 1096–1111. [CrossRef]
17. Wu, M.; Yu, S.; Wang, X.; Li, L. Ultra-high energy storage density and ultra-wide operating temperature range in $Bi_2Zn_{2/3}Nb_{4/3}O_7$ thin film as a novel lead-free capacitor. *J. Power Sources* **2021**, *497*, 229879. [CrossRef]
18. Li, X.; Zhang, J.; Liu, B.; Su, Z. A critical review on the application and recent developments of post-modified biochar in supercapacitors. *J. Clean. Prod.* **2021**, *310*, 127428. [CrossRef]
19. Liu, S.; Xu, Y.; Wu, J.; Huang, J. Huang Celery-derived porous carbon materials for superior performance supercapacitors. *Nanoscale Adv.* **2021**, *3*, 5363–5372. [CrossRef]
20. Liu, X.; Liu, L.; Yan, W.; Wang, Y.; Huang, C.; Wang, Z. Hierarchical Fe_3O_4@FeS_2 nanocomposite as high-specific-capacitance electrode material for supercapacitors. *Energy Technol.* **2020**, *8*, 2000544. [CrossRef]
21. Forouzandeh, P.; Kumaravel, V.; Pillai, S.C. Electrode materials for supercapacitors: A review of recent advances. *Catalysts* **2020**, *10*, 969. [CrossRef]
22. Abazari, R.; Sanati, S.; Morsali, A.; Dubal, D.P. High specific capacitance of a 3D-metal–organic framework-confined growth in $CoMn_2O_4$ nanostars as advanced supercapacitor electrode materials. *J. Mater. Chem. A* **2021**, *9*, 11001–11012. [CrossRef]
23. Xiong, S.; He, Y.; Zhang, X.; Wu, B.; Chu, J.; Wang, X.; Zhang, R.; Gong, M.; Li, Z.; Chen, Z. Hydrothermal synthesis of high specific capacitance electrode material using porous bagasse biomass carbon hosting MnO_2 nanospheres. *Biomass Convers. Biorefinery* **2021**, *11*, 1325–1334. [CrossRef]
24. Choudhary, N.; Li, C.; Moore, J.; Nagaiah, N.; Zhai, L.; Jung, Y.; Thomas, J. Asymmetric supercapacitor electrodes and devices. *Adv. Mater.* **2017**, *29*, 1605336. [CrossRef] [PubMed]
25. Guo, T.; Zhou, D.; Pang, L.; Sun, S.; Zhou, T.; Su, J. Perspectives on working voltage of aqueous supercapacitors. *Small* **2022**, *18*, 2106360. [CrossRef]

26. Song, F.; Ao, X.; Chen, Q. Effect of heteroatom doping on the charge storage and operating voltage window of nickel-based sulfide composite electrodes in alkaline electrolytes. *Chem. Eng. J.* **2022**, *427*, 130885. [CrossRef]
27. Gong, K.; Lee, H.; Choi, Y.; Jung, G.; Keum, K.; Kim, J.W.; Ha, J.S. A flexible supercapacitor with high energy density and wide range of temperature tolerance using a high-concentration aqueous gel electrolyte. *Electrochim. Acta* **2024**, *475*, 143585. [CrossRef]
28. nil Kumar, Y.; Yadav, A.A.; Al-Asbahi, B.A.; Kang, S.W.; Moniruzzaman, M. Sulfur nanoparticle-decorated nickel cobalt sulfide hetero-nanostructures with enhanced energy storage for high-performance supercapacitors. *Molecules* **2022**, *27*, 7458. [CrossRef] [PubMed]
29. Kadam, V.S.; Jagtap, C.V.; Lokhande, P.E.; Bulakhe, R.N.; Kang, S.W.; Yadav, A.A.; Pathan, H.M. One-step deposition of nanostructured $Ni(OH)_2$/rGO for supercapacitor applications. *J. Mater. Sci. Mater. Electron.* **2023**, *34*, 1083. [CrossRef]
30. Yadav, A.A.; Hunge, Y.M.; Ko, S.; Kang, S.W. Chemically synthesized iron-oxide-based pure negative electrode for solid-state asymmetric supercapacitor devices. *Materials* **2022**, *15*, 6133. [CrossRef]
31. Wang, J.; Chang, J.; Wang, L.; Hao, J. One-step and low-temperature synthesis of $CoMoO_4$ nanowire arrays on Ni foam for asymmetric supercapacitors. *Ionics* **2018**, *24*, 3967–3973. [CrossRef]
32. Ilayas, T.; Anjum, S.; Raja, M.Y.A.; Khurram, R.; Sattar, M.; Mansoor, A. Rietveld refinement, 3D view and electrochemical properties of rare earth lanthanum doped nickel ferrite to fabricate high performance electrodes for supercapacitor applications. *Ceram. Int.* **2023**, *49*, 28864–28877. [CrossRef]
33. Theerthagiri, J.; Durai, G.; Tatarchuk, T.; Sumathi, M.; Kuppusami, P.; Qin, J.; Choi, M.Y. Synthesis of hierarchical structured rare earth metal–doped Co_3O_4 by polymer combustion method for high performance electrochemical supercapacitor electrode materials. *Ionics* **2020**, *26*, 2051–2061. [CrossRef]
34. He, W.X.; Jiang, S.; Pang, M.G.; Li, J.W.; Pang, M.; Mao, M.M.; Wang, R.W.; Yang, H.; Pan, Q.L.; Zhao, J. A free-standing $NiMoO_4$@Mg-Co(OH)F core-shell nanocomposites supported on Ni foam for asymmetric supercapacitor applications. *Colloids Surf. A Physicochem. Eng. Asp.* **2023**, *660*, 130883. [CrossRef]
35. Wang, G.G.; Chen, Q.Y.; Zhang, J.; An, X.G.; Liu, Q.; Xie, L.S.; Yao, W.T.; Sun, X.P.; Kong, Q.Q. $NiMoO_4$ nanorods with oxygen vacancies self-supported on Ni foam towards high-efficiency electrocatalytic conversion of nitrite to ammonia. *J. Colloid Interface Sci.* **2023**, *647*, 73–80. [CrossRef] [PubMed]
36. Ren, B.; Wang, X.E.; Zhang, X.; Wang, B.; Li, Y.; Zeng, X.; Zhang, X.F.; Fan, M.Q.; Yang, X.D. Designed formation of hierarchical core-shell $NiCo_2S_4$@$NiMoO_4$ arrays on cornstalk biochar as battery-type electrodes for hybrid supercapacitors. *J. Alloys Compd.* **2023**, *937*, 168403. [CrossRef]
37. Sun, Y.S.; Liu, Z.Q.; Zheng, X.Z.; Wang, C.X.; Wang, J.H.; Jiang, M.Y.; Jiang, D.G.; Liu, J.Q. Construction of KCu_7S_4@$NiMoO_4$ three-dimensional core-shell hollow structure with high hole mobility and fast ion transport for high-performance hybrid supercapacitors. *Compos. Part B Eng.* **2023**, *249*, 110409. [CrossRef]
38. Chen, H.; Hu, H.; Han, F.; Liu, J.; Zhang, Y.; Zheng, Y. $CoMoO_4$/bamboo charcoal hybrid material for high-energy-density and high cycling stability supercapacitors. *Dalton Trans.* **2020**, *49*, 10799–10807. [CrossRef] [PubMed]
39. Fei, F.; Zhou, H.; Kang, M. POM-derived MoO_3/$CoMoO_4$ mixed oxides directed by glucose for high-performance supercapacitors. *New J. Chem.* **2022**, *46*, 16914–16921. [CrossRef]
40. Chen, C.; Deng, H.; Wang, C.; Luo, W.; Huang, D.; Jin, T. Petal-like $CoMoO_4$ clusters grown on carbon cloth as a binder-free electrode for supercapacitor application. *ACS Omega* **2021**, *6*, 19616–19622. [CrossRef]
41. Wang, J.; Hong, W.; Fu, Y. Urea-assisted synthesis of $CoMoO_4$–$NiMoO_4$ microspheres for the electrochemical energy storage. *Ionics* **2023**, *29*, 3077–3086. [CrossRef]

Disclaimer/Publisher's Note: The statements, opinions and data contained in all publications are solely those of the individual author(s) and contributor(s) and not of MDPI and/or the editor(s). MDPI and/or the editor(s) disclaim responsibility for any injury to people or property resulting from any ideas, methods, instructions or products referred to in the content.